


$B \rightarrow \rho \ell \bar{\nu}$ and $\omega \ell \bar{\nu}$ in and beyond the Standard Model: Improved predictions and $|V_{ub}|$

Florian U. Bernlochner¹, Markus T. Prim¹, and Dean J. Robinson²

¹*Physikalisches Institut der Rheinischen Friedrich-Wilhelms-Universität Bonn, 53115 Bonn, Germany*

²*Ernest Orlando Lawrence Berkeley National Laboratory, University of California, Berkeley, California 94720, USA*

 (Received 5 May 2021; accepted 15 July 2021; published 30 August 2021)

We revisit the experimental and theoretical status of $B \rightarrow \rho \ell \bar{\nu}$ and $B \rightarrow \omega \ell \bar{\nu}$ decays. We perform a combined fit of averaged spectra from Belle and BABAR measurements with prior light-cone sum rule calculations in order to obtain more precise predictions over the full q^2 range. The extracted values of $|V_{ub}|$ from these combined fits exhibit smaller uncertainty compared to previous extractions from $B \rightarrow \rho \ell \bar{\nu}$ and $B \rightarrow \omega \ell \bar{\nu}$ decays, and the central values are found to be smaller than values extracted from $B \rightarrow \pi \ell \bar{\nu}$ or inclusive measurements. We use our fit results to obtain more precise predictions in and beyond the Standard Model for the lepton universality ratios $R(\rho)$ and $R(\omega)$, as well as several angular observables that are sensitive to the full q^2 distribution, such as the longitudinal polarization of the vector meson, the τ polarization, and its forward-backward asymmetry.

DOI: 10.1103/PhysRevD.104.034032

I. INTRODUCTION

Semileptonic decays offer a clean laboratory to search for physical phenomena beyond those predicted by the Standard Model (SM) of particle physics. Intriguingly, semitaquonic transitions involving charmed final states—i.e., $b \rightarrow c \tau \bar{\nu}$ decays—show a persistent lepton flavor universality violation (LFUV) anomaly at the 3σ level [1] or higher when various decay modes are combined; see Ref. [2] for a recent review. As pointed out by, e.g., Refs. [3–5], semitaquonic transitions involving charmless hadronic final states offer an intriguing independent probe of LFUV anomalies. In particular, exploring $b \rightarrow u \tau \bar{\nu}$ decays can be a sensitive probe of the flavor structure of new physics (NP) mediators (if any) responsible for the $b \rightarrow c \tau \bar{\nu}$ LFUV anomalies. For instance, if the same NP were present in $b \rightarrow u$ semitaquonic decays as in $b \rightarrow c$ semitaquonic decays, one would naively expect LFUV deviations from the SM in the former to be enhanced by $|V_{cb}|^2/|V_{ub}|^2 \sim 10^2$ compared to the $\sim 10\%$ – 20% LFUV excess rates seen in $b \rightarrow c \tau \bar{\nu}$.

In 2015, Belle published the first search for $B \rightarrow \pi \tau \bar{\nu}$ using single-prong hadronic and leptonic τ decays [6]. Their measured upper limit of the branching fraction can be translated into a C.L. for the ratio of semitaquonic and light-lepton modes [3], i.e., the lepton universality ratio

$$R(\pi) = \frac{\Gamma(B \rightarrow \pi \tau \bar{\nu})}{\Gamma(B \rightarrow \pi \ell \bar{\nu})} = 1.05 \pm 0.51, \quad (1)$$

with $\ell = e$ or μ . The measured value is compatible with the SM predictions $R(\pi)_{\text{SM}} = 0.641 \pm 0.016$ [3] or 0.688 ± 0.014 [5]. It is expected that Belle II will discover this decay, and then push its measured precision to the 5%–6% level with the anticipated full dataset [2].

In this paper, we explore $B \rightarrow \rho \tau \bar{\nu}$ and $B \rightarrow \omega \tau \bar{\nu}$ transitions (collectively denoted $B \rightarrow V \tau \bar{\nu}$). Measurements of $B \rightarrow V \tau \bar{\nu}$ decays feature several advantages over $B \rightarrow \pi \tau \bar{\nu}$ in terms of their potential sensitivity to NP effects, including an increased branching fraction with respect to the pion final state, and a larger set of angular observables from the subsequent $\rho \rightarrow \pi \pi$ and $\omega \rightarrow \pi \pi \pi$ decays that may probe NP effects arising in the polarization of the ρ and ω . The Belle II experiment has started recording its first collision data: Large and clean datasets of these final states will soon be available to probe the full differential information in these decays. In addition, LHCb has established itself as a source of precise measurements of semileptonic processes. With its sizeable datasets, it is conceivable that its first measurements of $b \rightarrow u \tau \bar{\nu}$ transitions will appear in the near future, with $B^+ \rightarrow \rho^0 \tau^+ \bar{\nu}$ and $\Lambda_b \rightarrow p \tau \bar{\nu}$ being likely candidates.

To produce reliable $B \rightarrow V \tau \bar{\nu}$ predictions for both the SM and NP, in this paper we reanalyze the available experimental measurements of the differential decay rates in q^2 for $B \rightarrow \rho \ell \bar{\nu}$ and $B \rightarrow \omega \ell \bar{\nu}$ published by BABAR [7,8] and Belle [9]. Newly averaged spectra are obtained, following the prescription utilized by HFLAV

Published by the American Physical Society under the terms of the Creative Commons Attribution 4.0 International license. Further distribution of this work must maintain attribution to the author(s) and the published article's title, journal citation, and DOI. Funded by SCOAP³.

where $q = p_B - p_V$. The Clebsch-Gordan coefficient takes the value $c_V = 1/\sqrt{2}$ for the neutral unflavored meson final states $V = \rho^0$ and ω^0 , while $c_V = 1$ for ρ^\pm . For each current $\bar{u}\Gamma b$, the T_i^Γ denote a basis of the allowed amplitudes—tensors of the involved 4-momenta and polarizations—while F_i^Γ are their corresponding form factors. In $B \rightarrow V$ transitions there are a total of eight possible independent amplitudes, and hence eight form factors. As in Ref. [11], we choose the basis $\{A_P, V, A_0, A_1, A_{12}, T_1, T_2, T_{23}\}$ defined explicitly via²

$$\langle V | \bar{u} \gamma^5 b | \bar{B} \rangle = c_V A_P \varepsilon^* \cdot q, \quad (6a)$$

$$\langle V | \bar{u} \gamma^\mu b | \bar{B} \rangle = \frac{ic_V V \varepsilon^{\mu\nu\rho\sigma} \varepsilon_\nu^* (p_B + p_V)_\rho q_\sigma}{m_B + m_V}, \quad (6b)$$

$$\begin{aligned} \langle V | \bar{u} \gamma^\mu \gamma^5 b | \bar{B} \rangle = c_V \bigg\{ & A_1 (m_B + m_V) \varepsilon^{*\mu} \\ & - A_2 \frac{(p_B + p_V)^\mu \varepsilon^* \cdot q}{m_B + m_V} \\ & + \frac{\varepsilon^* \cdot q q^\mu}{q^2} [A_2 (m_B - m_V) \\ & - A_1 (m_B + m_V) + 2m_V A_0] \bigg\}, \quad (6c) \end{aligned}$$

$$\begin{aligned} \langle V | \bar{u} \sigma^{\mu\nu} b | \bar{B} \rangle = -c_V \varepsilon^{\mu\nu\rho\sigma} \bigg\{ & T_1 \varepsilon_\rho^* (p_B + p_V)_\sigma \\ & - (T_2 + T_1) \frac{m_B^2 - m_V^2}{q^2} \varepsilon_\rho^* q_\sigma \\ & + (p_B + p_V)_\rho q_\sigma \frac{\varepsilon^* \cdot q}{q^2} [(T_1 + T_2) \\ & + T_3 \frac{q^2}{m_B^2 - m_V^2}] \bigg\}, \quad (6d) \end{aligned}$$

with the additional redefinitions with respect to A_{12} and T_{23} ,

$$4|p_V|^2 m_B^2 A_2 = A_1 (m_B^2 - m_V^2 - q^2) (m_B + m_V)^2 - 16A_{12} m_B m_V^2 (m_B + m_V), \quad (7a)$$

$$4|p_V|^2 m_B^2 T_3 = T_2 (m_B^2 + 3m_V^2 - q^2) (m_B^2 - m_V^2) - 8T_{23} m_B m_V^2 (m_B - m_V). \quad (7b)$$

Here, m_B (m_V) is the mass of the B (vector) meson, and $|p_V|$ denotes the vector meson 3-momentum in the B rest frame,

²It is perhaps unfortunate that the notation for the vector form factor $V = V(q^2)$ is identical to the notation for the vector meson, V . Whether the vector meson or the vector form factor is meant will always be clear from context.

$$\begin{aligned} |p_V| &= m_V \sqrt{w^2 - 1}, \\ &= \sqrt{\lambda(q^2)} / (2m_B), \quad w = \frac{m_B^2 + m_V^2 - q^2}{2m_B m_V} \end{aligned} \quad (8)$$

in which the Källén function $\lambda(q^2) = [(m_B + m_V)^2 - q^2][(m_B - m_V)^2 - q^2]$. Note, $\langle V | \bar{u} b | \bar{B} \rangle = 0$ by angular momentum and parity conservation. The identity $\sigma^{\mu\nu} \gamma^5 \equiv -(i/2) \varepsilon^{\mu\nu\rho\sigma} \sigma_{\rho\sigma}$ corresponding to $\text{Tr}[\gamma^\mu \gamma^\nu \gamma^\sigma \gamma^\rho \gamma^5] = +4i \varepsilon^{\mu\nu\rho\sigma}$ allows one to write down the matrix element for the axial-tensor current $\langle V | \bar{u} \sigma^{\mu\nu} \gamma^5 b | \bar{B} \rangle$ from the tensor (6d). This is the standard Lorentz sign convention in the $B \rightarrow D^*$ literature. One may instead choose the sign conventions such that $\sigma^{\mu\nu} \gamma^5 \equiv +(i/2) \varepsilon^{\mu\nu\rho\sigma} \sigma_{\rho\sigma}$ corresponding to the more common $\text{Tr}[\gamma^\mu \gamma^\nu \gamma^\sigma \gamma^\rho \gamma^5] = -4i \varepsilon^{\mu\nu\rho\sigma}$. In this case, the sign of the vector and tensor currents in Eqs. (6b) and (6d) also changes.

The construction of the form factor basis in Eqs. (6) assumes the vector meson V may be treated as an on-shell state. While a good assumption for the narrow ω^0 , this is a poorer assumption for the relatively broad ρ ; cf. Ref. [25]. For instance, once subsequent $\rho \rightarrow \pi\pi$ decays are considered, longitudinal modes may generate important contributions naively $\sim (1 - p_V^2/m_V^2) \sim \Gamma_V/m_V$; recent analyses of $B \rightarrow \pi\pi$ form factors suggest finite-width corrections could be as large as 20% [26]. In a sufficiently narrow range of p_V^2 near the ρ pole, such effects are always subleading, albeit at the expense of a smaller branching ratio. Such finite-width effects, however, are typically not considered in experimental analyses, which instead simulate such processes using the narrow-width approximation with a finite-width Γ_ρ , and permit the $\pi\pi$ invariant mass to fall within a relatively broad range, $|m_{\pi\pi} - m_\rho| \lesssim \Gamma_\rho$ [7] or $2\Gamma_\rho$ [9]. Additionally, interference effects with nonresonant $B \rightarrow \pi\pi \ell \bar{\nu}_\ell$ production are neglected. We shall therefore do the same here, fixing the end point of the q^2 range to (be close to) the usual $(m_B - m_\rho)^2$, and neglecting the impact of nonresonant $B \rightarrow \pi\pi \ell \bar{\nu}_\ell$ production on the predicted rates: The impact of such contributions in light leptons was recently measured for the first time in Ref. [27], which reported the full sum of resonant and nonresonant semi-leptonic dipion final states, i.e., the sum of ρ , higher resonant states, as well as nonresonant $\pi\pi$ contributions. We note that our final result for $|V_{ub}|$ from $B \rightarrow \rho \ell \bar{\nu}$ [see Eq. (24) below] using data that assumes a narrow-width approximation is in excellent agreement with that from the decay to the much narrower ω .

In Appendix A, we provide the explicit forms of the $B \rightarrow V l \bar{\nu}$ helicity amplitudes for all SM and NP couplings, as well as the amplitudes and full differential rates once subsequent $\rho \rightarrow \pi\pi$ or $\omega \rightarrow \pi\pi\pi$ decays are included. For the purposes of our fit below, it is enough to present here just the SM amplitudes and differential rate for $B \rightarrow V l \bar{\nu}$. NP effects are discussed further in Sec. V. In the standard

helicity basis, the $B \rightarrow V\ell\bar{\nu}$ helicity amplitudes take the form (up to an overall unphysical phase; see Appendix A)

$$H_{\pm}(q^2) = \frac{2m_B|p_V|V(q^2)}{m_B + m_V} \pm (m_B + m_V)A_1(q^2), \quad (9a)$$

$$H_0(q^2) = 8m_B m_V A_{12}(q^2) / \sqrt{q^2}, \quad (9b)$$

$$H_s(q^2) = 2m_B|p_V|A_0(q^2) / \sqrt{q^2}. \quad (9c)$$

The SM differential rate is then given by

$$\begin{aligned} \frac{d\Gamma}{dq^2} &= \frac{G_F^2 |V_{ub}|^2 c_V^2}{96\pi^3} |p_V| \frac{q^2}{m_B^2} \left(1 - \frac{m_\ell^2}{q^2}\right)^2 \\ &\times \left\{ \left[1 + \frac{m_\ell^2}{2q^2}\right] (H_+^2(q^2) + H_-^2(q^2) + H_0^2(q^2)) \right. \\ &\left. + \frac{3m_\ell^2}{2q^2} H_s^2(q^2) \right\}. \quad (10) \end{aligned}$$

In line with the approach of the $B \rightarrow \pi\ell\bar{\nu}$ analysis of Ref. [1], the electroweak correction [28] for semileptonic decays $\eta_{EW} = 1 + (\alpha/\pi) \log(m_Z/m_B) \approx 1.0066$ is not included in the rate. This correction can always be applied *post facto* using the transformation $|V_{ub}| \rightarrow |V_{ub}|\eta_{EW}$. Additional long-distance QED corrections may further affect the determined value of $|V_{ub}|$. These corrections have been estimated to be small using a scalar QED approximation with some model assumptions [29] (see also Ref. [30]). In the massless lepton limit, the scalar helicity amplitude H_s , and hence A_0 , does not contribute, reducing the SM form factors to three. The “zero mass approximation”—neglecting the electron or muon mass—is used in Secs. III and IV below to obtain fits for V , A_1 , and A_{12} .

The form factors themselves are hadronic functions that cannot be determined with perturbative methods, since they incorporate nonperturbative QCD effects. However, one may exploit dispersion relations plus analyticity and unitarity bounds to parametrize them in a model-independent manner. Similar to the Boyd-Grinstein-Lebed parametrization for $B \rightarrow D^{(*)}$ [31,32], the Bourrely-Caprini-Lellouch (BCL) parametrization [33] exploits a dispersive approach to express the (originally $B \rightarrow \pi$) form factors as a power expansion with respect to the conformal parameter

$$z(q^2, t_0) = \frac{\sqrt{t_+ - q^2} - \sqrt{t_+ - t_0}}{\sqrt{t_+ - q^2} + \sqrt{t_+ - t_0}}. \quad (11)$$

Here the pair production threshold $t_+ = (m_B + m_V)^2$ and the z origin is determined by the optimized choice $t_0 = (m_B + m_V)(\sqrt{m_B} - \sqrt{m_V})^2$ that minimizes the range of $|z|$ to be ≤ 0.10 . (BCL further applies a constraint on the

gradient of the $B \rightarrow \pi$ vector form factor at $z = -1$.) Naive regularization of the $1/q^2$ terms in Eqs. (6c) and (6d) implies the kinematic relations at $q^2 = 0$,

$$A_0(0) = \frac{8m_B m_V A_{12}(0)}{m_B^2 - m_V^2}, \quad T_1(0) = T_2(0). \quad (12)$$

The BSZ parametrization [11] modifies the BCL parametrization by reorganizing the power expansion in z as a “simplified series expansion” about $q^2 = 0$ in order to straightforwardly impose these relations at zeroth order. That is, the form factors are expanded as

$$F_i(q^2) = P_i(q^2) \sum_k \alpha_k^i (z(q^2) - z(0))^k. \quad (13)$$

Just as for BCL, for each current a single subthreshold resonance is assumed at $q^2 = m_R^2$, such that the (inverse) Blaschke factor $P_i(q^2) = (1 - q^2/m_R^2)^{-1}$. As allowed by angular momentum and parity, these resonances are explicitly for each of the form factors

$$\begin{aligned} A_P, A_0: & \quad R = B, & m_B &\simeq 5.279 \text{ GeV}, \\ V, T_1: & \quad R = B^*, & m_{B^*} &\simeq 5.325 \text{ GeV}, \\ A_{1,12}, T_{2,23}: & \quad R = B_1, & m_{B_1} &\simeq 5.724 \text{ GeV} \end{aligned}$$

coupling to $J^P = 0^-, 1^-,$ and 1^+ partial waves, respectively. Finally, the quark equations of motion may be used to relate the pseudoscalar form factor A_P to A_0 via

$$A_P = -\frac{2m_V}{m_b + m_u} A_0. \quad (14)$$

Here, $m_{b,u}$ are formally scheme-dependent quantities. The BSZ parametrization [11] uses the pole mass scheme, with explicitly $m_b \simeq 4.8$ GeV, and the much lighter u quark mass is neglected. We use the same scheme.

Because of the unstable nature of the ρ and ω mesons, lattice QCD (LQCD) predictions are challenging, and so far have not yet provided predictions with controlled systematic uncertainties that may be used in fits with data [34]. One may instead exploit LCSR [35–38] predictions for these transitions [11,26,39,40], which are typically applicable in the low q^2 regime, $q^2 \lesssim \mathcal{O}(m_b \Lambda_{\text{QCD}}) \sim 14$ GeV. In particular, we make use of the LCSR fit results for the BSZ parameters [11] comprising a fit to quadratic order in $z(q^2) - z(0)$. These results are shown in Table I. (For $b \rightarrow s$ transitions, Ref. [11] also quotes combined fits of LCSR predictions with LQCD results, which are available for those decays.)

Importantly, the LCSR themselves generate correlated predictions between SM and NP form factors. Thus, fitting these predictions in combination with measurements of the q^2 spectra for $B \rightarrow V\ell\bar{\nu}$, in which only SM contributions

TABLE I. LCSR prediction for the BSZ parameters in semi-leptonic $B \rightarrow \rho$ and $B \rightarrow \omega$ transitions. The full correlation matrices are given in [11]. Note, $\alpha_0^{A_0}$ and $\alpha_0^{T_2}$ are fixed with respect to $\alpha_0^{A_{1,2}}$ and $\alpha_0^{T_1}$, respectively, by the relations at $q^2 = 0$ (12).

Parameter	$B \rightarrow \rho$	$B \rightarrow \omega$
$\alpha_1^{A_0}$	-0.83 ± 0.20	-0.83 ± 0.30
$\alpha_2^{A_0}$	1.33 ± 1.05	1.42 ± 1.25
$\alpha_0^{A_1}$	0.26 ± 0.03	0.24 ± 0.03
$\alpha_1^{A_1}$	0.39 ± 0.14	0.34 ± 0.24
$\alpha_2^{A_1}$	0.16 ± 0.41	0.09 ± 0.57
$\alpha_0^{A_{12}}$	0.30 ± 0.03	0.27 ± 0.04
$\alpha_1^{A_{12}}$	0.76 ± 0.20	0.66 ± 0.26
$\alpha_2^{A_{12}}$	0.46 ± 0.76	0.28 ± 0.98
α_0^V	0.33 ± 0.03	0.30 ± 0.04
α_1^V	-0.86 ± 0.18	-0.83 ± 0.29
α_2^V	1.80 ± 0.97	1.72 ± 1.24
$\alpha_0^{T_1}$	0.27 ± 0.03	0.25 ± 0.03
$\alpha_1^{T_1}$	-0.74 ± 0.14	-0.72 ± 0.22
$\alpha_2^{T_1}$	1.45 ± 0.77	1.41 ± 1.01
$\alpha_0^{T_2}$	0.47 ± 0.13	0.41 ± 0.23
$\alpha_1^{T_2}$	0.58 ± 0.46	0.46 ± 0.57
$\alpha_2^{T_2}$	0.75 ± 0.08	0.68 ± 0.09
$\alpha_0^{T_{23}}$	1.90 ± 0.43	1.65 ± 0.62
$\alpha_1^{T_{23}}$	2.93 ± 1.81	2.47 ± 2.19

are assumed, nonetheless allows for predictions of improved precision for both the SM and NP $B \rightarrow V$ form factors. We proceed to perform such fits in Sec. IV.

III. BELLE AND BABAR SPECTRUM AVERAGES

As a first step of our study, we generate averaged q^2 spectra from the measurements performed by the Belle and BABAR experiments [7–9]. To do this, we note the $B \rightarrow \rho \ell \bar{\nu}$ measurements of Belle and BABAR have a compatible binning, which allows one to straightforwardly create an averaged differential spectrum. We define a χ^2 function of the form

$$\chi^2(\bar{\mathbf{x}}) = \sum_{m \in \{\text{Belle}, \text{BABAR}\}} \Delta \mathbf{y}_m^T \mathbf{C}_m^{-1} \Delta \mathbf{y}_m,$$

$$\Delta \mathbf{y}_m = \begin{pmatrix} \vdots \\ x_i^m - \sum_{j>N_{i-1}}^{N_i} \bar{x}_j \\ \vdots \end{pmatrix}, \quad (15)$$

where \mathbf{C}_m is the covariance of the measurement and x_i^m is the measured differential rate in bin i multiplied by the corresponding bin width. Further, $\bar{\mathbf{x}}$ denotes the averaged spectrum and $(N_{i-1}, N_i]$ the range of averaged bins used to

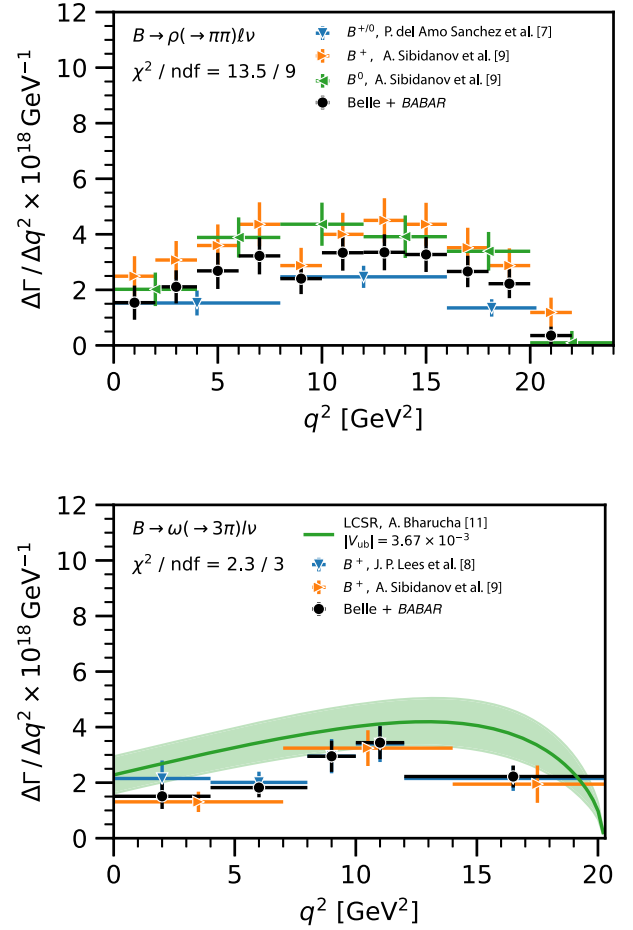


FIG. 1. The averaged q^2 spectrum of the measurements listed in the text for the ρ (top) and ω (bottom) final state on top of the latest Belle and BABAR measurements. The isospin transformation is applied to the $B^0 \rightarrow \rho^- \ell^+ \nu$ measurements. In the bottom figure, we also show the model (green band) which was used to split the bins in the averaging procedure.

map to the i th measured bin. The binning of the averaged spectrum is chosen to match the most granular spectrum. The averaged spectrum is shown in black in Fig. 1 and tabulated in Table II.

For the average of the $B \rightarrow \omega \ell \bar{\nu}$ measurements from Belle and BABAR, we again chose the binning of the most granular spectrum, in this case BABAR’s. However the experimental spectra do not have a compatible binning in terms of matching bin boundaries. In order to incorporate the Belle data and create an averaged spectrum, the LCSR fit results [11] are used to create a model with which to split the second and fifth bin of the chosen binning shown in black in Fig. 1. To match the average bin onto a measurement without matching bin edges, the average bin \bar{x}_i , $i = 2$ or 5 is split into two parts delimited by the lower bin edge, the q^2 value where the bin is split, and the upper bin edge. We label the two parts of the split bin as “left” and “right,” respectively, in the following and define

TABLE II. Averaged spectra. For the corresponding correlation matrices, see Tables VI and VII.

$B \rightarrow \rho \ell \bar{\nu}$	
q^2 bin	$\Delta\Gamma/\Delta q^2 \times 10^6$
[0, 2]	1.54 ± 0.62
[2, 4]	2.11 ± 0.60
[4, 6]	2.68 ± 0.65
[6, 8]	3.22 ± 0.67
[8, 10]	2.40 ± 0.56
[10, 12]	3.34 ± 0.65
[12, 14]	3.35 ± 0.65
[14, 16]	3.27 ± 0.63
[16, 18]	2.66 ± 0.57
[18, 20]	2.22 ± 0.52
[20, 22]	0.35 ± 0.32
$B \rightarrow \omega \ell \bar{\nu}$	
q^2 bin	$\Delta\Gamma/\Delta q^2 \times 10^6$
[0, 4]	1.51 ± 0.46
[4, 8]	1.82 ± 0.35
[8, 10]	2.95 ± 0.56
[10, 12]	3.44 ± 0.59
[12, 21]	2.22 ± 0.40
Nuisance parameters	
θ_2	-0.01 ± 1.00
θ_5	0.00 ± 1.00

$$\begin{aligned}\bar{x}_{i,\text{left}} &= I_{i,\text{left}}/I_i(1 + \theta_i \varepsilon_{i,\text{left}}), \\ \bar{x}_{i,\text{right}} &= I_{i,\text{right}}/I_i(1 - \theta_i \varepsilon_{i,\text{right}}),\end{aligned}\quad (16)$$

where $I_{i,\text{left}}$ ($I_{i,\text{right}}$) is the integral of the model function on the support of the left (right) part of the split bin, the sum $I_i = I_{i,\text{left}} + I_{i,\text{right}}$ is the integral over the entire bin, $\varepsilon_{i,\text{left}}$ ($\varepsilon_{i,\text{right}}$) the uncertainty of the integration given by the model uncertainty, and θ_i the nuisance parameter for the model dependence. We point out that the averaged spectrum does not depend on $|V_{\text{ub}}|$, as $|V_{\text{ub}}|$ cancels in the ratios $I_{i,\text{left}}/I_i$ ($I_{i,\text{right}}/I_i$). The averaged spectrum is shown in black in Fig. 1 and tabulated in Table II. The result is almost independent of the nuisance parameters, as can be seen in

TABLE III. Averaged total branching ratio with $\tau_{B^+} = 1.638 \times 10^{-12}$ s and the total rate given by the sum over the bins of the averaged spectra. The discrepancy between our result and the PDG arises because of the method of averaging. The PDG averages the directly measured branching ratios, whereas we average the provided unfolded spectra.

Decay	Branching ratio ($\times 10^{-4}$)	
	Our result	PDG
$B^+ \rightarrow \rho^0 \ell \nu$	1.35 ± 0.12	1.58 ± 0.11
$B^+ \rightarrow \omega \ell \nu$	1.14 ± 0.13	1.19 ± 0.09

the correlation matrix of the fit. The averaged total branching ratios, defined as the sum over the spectrum, are given in Table III. We find a slight discrepancy with previous averages, which can be explained by the averaging procedure.

IV. COMBINED DATA AND THEORY FIT

We now fit the LCSR results in Table I combined with the averaged spectra in Sec. III over the whole q^2 region, thereby generating new predictions for the BSZ parameters beyond the $q^2 \lesssim 14$ GeV² regime of validity for the LCSR results. To this end, we define a χ^2 function of the form

$$\begin{aligned}\chi^2(|V_{\text{ub}}|, \mathbf{c}) &= \Delta \mathbf{c}^T \mathbf{C}_{\text{LCSR}}^{-1} \Delta \mathbf{c} + \Delta \mathbf{y}^T \mathbf{C}_{\text{Spectrum}}^{-1} \Delta \mathbf{y}, \\ \Delta \mathbf{c} &= \mathbf{c}_{\text{LCSR}} - \mathbf{c}, \\ \Delta \mathbf{y} &= \mathbf{y}_{\text{Spectrum}} - \Delta \Gamma(V_{\text{ub}}, \mathbf{c})/\Delta q^2.\end{aligned}\quad (17)$$

Here, \mathbf{c} denotes the vector of BSZ parameters and \mathbf{y} is the binned differential decay rate. Note that $|V_{\text{ub}}|$ is included in the χ^2 function and fitted simultaneously with the BSZ expansion coefficients. We minimize the χ^2 function using sequential least squares programming: The result of the fit is tabulated in Tables IV, VIII, and IX. The differential rates for the leptonic and taonic mode for both decays using our fitted coefficients are shown in Fig. 2.

We perform several cross-checks of our final fit. First, instead of a combined fit using the averaged spectrum

TABLE IV. Fit result for $|V_{\text{ub}}|$ and the BCL expansion coefficients. The corresponding correlation matrices can be found in Tables VIII and IX.

Parameter	$B \rightarrow \rho$	$B \rightarrow \omega$
$ V_{\text{ub}} $	2.96 ± 0.29	2.99 ± 0.35
$\alpha_1^{A_0}$	-0.86 ± 0.19	-0.94 ± 0.28
$\alpha_2^{A_0}$	1.43 ± 1.02	1.78 ± 1.20
$\alpha_0^{A_1}$	0.26 ± 0.03	0.24 ± 0.03
$\alpha_1^{A_1}$	0.38 ± 0.13	0.30 ± 0.22
$\alpha_2^{A_1}$	0.16 ± 0.41	0.00 ± 0.55
$\alpha_0^{A_{12}}$	0.29 ± 0.03	0.25 ± 0.04
$\alpha_1^{A_{12}}$	0.72 ± 0.17	0.54 ± 0.24
$\alpha_2^{A_{12}}$	0.37 ± 0.70	-0.03 ± 0.96
α_0^V	0.33 ± 0.03	0.31 ± 0.04
α_1^V	-0.87 ± 0.18	-0.89 ± 0.27
α_2^V	1.88 ± 0.94	1.81 ± 1.19
$\alpha_0^{T_1}$	0.27 ± 0.03	0.25 ± 0.03
$\alpha_1^{T_1}$	-0.75 ± 0.14	-0.76 ± 0.21
$\alpha_2^{T_1}$	1.51 ± 0.76	1.50 ± 0.96
$\alpha_1^{T_2}$	0.46 ± 0.13	0.37 ± 0.21
$\alpha_2^{T_2}$	0.59 ± 0.46	0.38 ± 0.55
$\alpha_0^{T_{23}}$	0.74 ± 0.07	0.65 ± 0.09
$\alpha_1^{T_{23}}$	1.83 ± 0.40	1.40 ± 0.58
$\alpha_2^{T_{23}}$	2.88 ± 1.79	2.03 ± 2.18

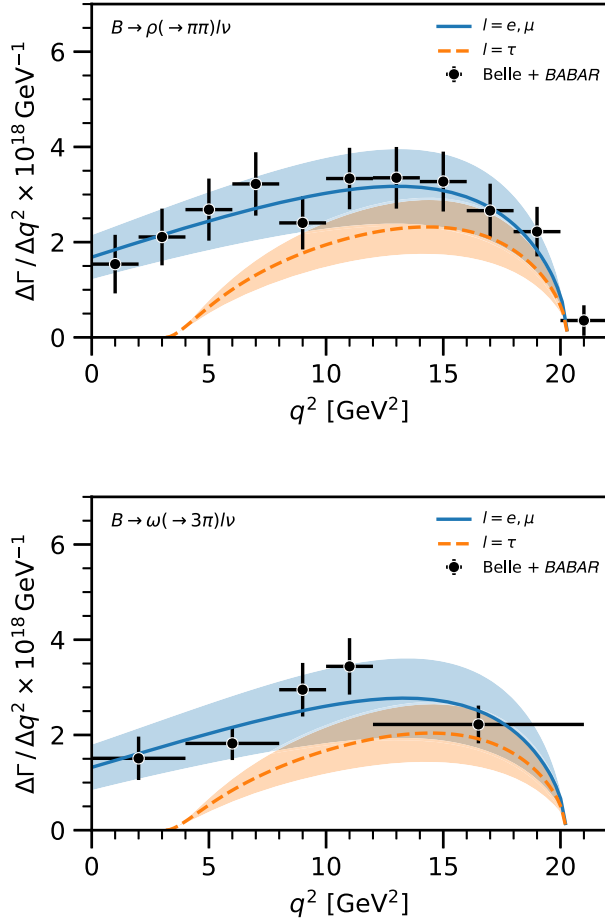


FIG. 2. The differential decay rates for the leptonic and taonic mode with our fit result for the BSZ coefficients for $B \rightarrow \rho l\bar{\nu}$ (top) and $B \rightarrow \omega l\bar{\nu}$ (bottom).

described in Sec. III, we performed the fit with the individual spectra provided by the experiments. Second, the impact of the tensor form factors via their correlations to the nontensor form factors was studied by fitting only the (SM) parameters contributing to the light-lepton final state. Third, we sampled the form factors at different $q^2 = 0, 7, 14 \text{ GeV}^2$ from a multidimensional Gaussian distribution, with mean and covariance set by the LCSR results and incorporated these into the χ^2 function. For each of these three cross-checks, no significant differences with respect to our combined fit results were found. This provides good evidence that our treatment of the form factors in the fit does not bias the result. The fit results for both final states are shown in Fig. 2.

We find that the extracted $|V_{ub}|$ is consistently smaller in comparison to the extraction from $B \rightarrow \pi l\bar{\nu}$ decays. Our extracted values for $|V_{ub}|$ are compatible with the extractions in Ref. [11], but yield lower uncertainties, because we extract $|V_{ub}|$ from a combination of experiments and LCSR results over the full q^2 range instead of individually for the Belle and BABAR experiments with different q_{max}^2 cutoffs. As a cross-check, we have repeated the fit with different cutoffs of the measured q^2 spectrum. The results of these fits are shown

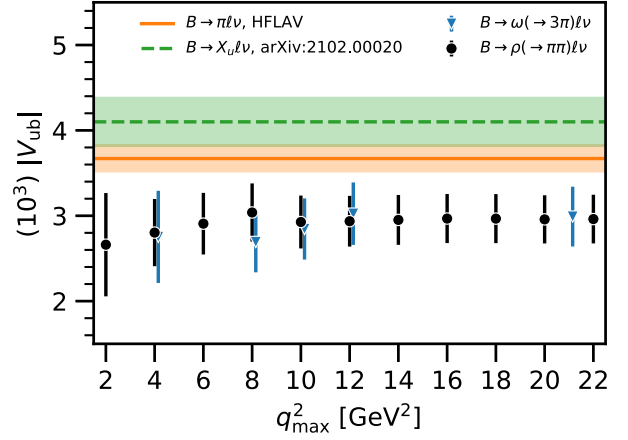


FIG. 3. The extracted $|V_{ub}|$ values from $B \rightarrow \rho l\bar{\nu}$ and $B \rightarrow \omega l\bar{\nu}$ for different cutoffs q_{max}^2 of the respective q^2 spectrum in the fit. The stable extraction of V_{ub} for increasing q^2 cutoffs indicates that the extrapolation into the high q^2 region works.

in Fig. 3. We consistently find central values for $|V_{ub}|$ from $B \rightarrow \rho l\bar{\nu}$, and $B \rightarrow \omega l\bar{\nu}$ below the value for $|V_{ub}|$ extracted from $B \rightarrow \pi l\bar{\nu}$. The stable $|V_{ub}|$ extraction for increasing q^2 cutoffs indicates that the extrapolation of the form factors into the high q^2 region is reliable. We also perform the fits to extract $|V_{ub}|$ for each experiment separately due to the large discrepancy in the measured $B \rightarrow \rho l\bar{\nu}$ spectra between Belle and BABAR. The results of these individual fits are summarized in Fig. 4. We find that for the ρ channel, the measurements of Belle and BABAR exhibit a slight tension.

V. PREDICTIONS IN THE STANDARD MODEL AND BEYOND

Using our combined fit, in Table V we provide SM predictions for the lepton universality ratios $R(\rho)$ and $R(\omega)$ defined as usual as

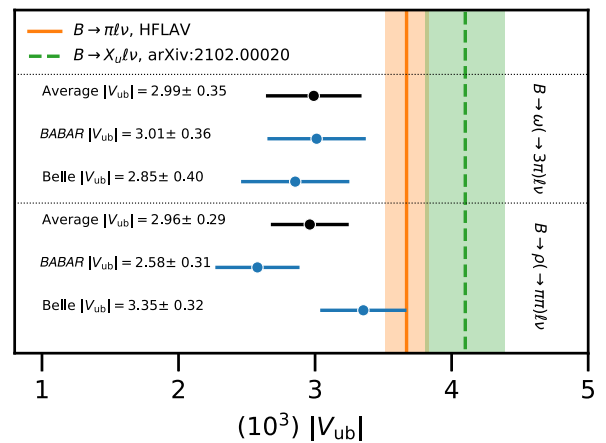


FIG. 4. The extracted $|V_{ub}|$ values from $B \rightarrow \rho l\bar{\nu}$ and $B \rightarrow \omega l\bar{\nu}$ for the fits to the individual experiments, and our averaged spectra. The $B \rightarrow \rho l\bar{\nu}$ measurements of Belle and BABAR exhibit a slight tension.

$$R(V) = \frac{\Gamma(B \rightarrow V\tau\bar{\nu})}{\Gamma(B \rightarrow V\ell\bar{\nu})}. \quad (18)$$

The combined fit improves the prediction for these observables over using the LCSR fit results alone by 24% and 13%, respectively. It is further interesting to consider phase space constrained lepton universality ratios, as pointed out by Refs. [41,42],

$$\tilde{R}(V) = \frac{\int_{m_\tau^2}^{t_-} dq^2 [d\Gamma(B \rightarrow V\tau\bar{\nu})/dq^2]}{\int_{m_\tau^2}^{t_-} dq^2 [d\Gamma(B \rightarrow V\ell\bar{\nu})/dq^2]}, \quad (19)$$

i.e., restricting the light-lepton mode to $m_\tau^2 \leq q^2 \leq (m_B - m_V)^2 \equiv t_-$, such that the phase space suppression of the τ mode is lifted. In $\tilde{R}(V)$, the correlation is increased between the nominator and denominator, and thus a larger cancellation of uncertainties is possible, but a small dependence on the actual shape of the light-lepton differential rate is introduced by the cutoff at m_τ^2 . $\tilde{R}(V)$ is insensitive to the low $q^2 \leq m_\tau^2 \simeq 3.16$ GeV² regime, reducing its sensitivity to data in the nominal regime of validity of the light-cone expansion $q^2 \lesssim 14$ GeV². However, we see in Table V that the LCSR predictions for $\tilde{R}(\rho)$ and $\tilde{R}(\omega)$ are in good agreement with the combined fit, suggesting that the experimental data do not pull the (extrapolation of the) LCSR fit results significantly in the higher q^2 regime.

We also calculate SM predictions for several angular observables, utilizing our combined fit result for the form factors. First, we consider the vector meson longitudinal polarization fraction

TABLE V. Predictions for the taonic-to-leptonic ratios $R(V)$, $\tilde{R}(V)$, the longitudinal fractions F_L , the τ polarization, and the forward-backward asymmetries using the LCSR predictions and our combined fit results for the BSZ parameters.

	LCSR [11]	Fit	Improvement
$R(\rho)$	0.532 ± 0.011	0.535 ± 0.009	24%
$\tilde{R}(\rho)$	0.605 ± 0.007	0.606 ± 0.007	4%
$F_{L,\ell}(\rho)$	0.512 ± 0.068	0.498 ± 0.058	15%
$F_{L,\tau}(\rho)$	0.496 ± 0.062	0.482 ± 0.052	16%
$P_\tau(\rho)$	0.543 ± 0.025	0.552 ± 0.020	21%
$A_{\text{FB},\ell}(\rho)$	-6.641 ± 0.769	-6.773 ± 0.644	16%
$A_{\text{FB},\tau}(\rho)$	-2.023 ± 0.705	-2.214 ± 0.615	13%
$R(\omega)$	0.534 ± 0.018	0.543 ± 0.015	13%
$\tilde{R}(\omega)$	0.606 ± 0.012	0.610 ± 0.011	5%
$F_{L,\ell}(\omega)$	0.501 ± 0.071	0.472 ± 0.067	6%
$F_{L,\tau}(\omega)$	0.486 ± 0.069	0.465 ± 0.065	5%
$P_\tau(\omega)$	0.545 ± 0.029	0.554 ± 0.028	2%
$A_{\text{FB},\ell}(\omega)$	-6.604 ± 0.868	-7.015 ± 0.852	2%
$A_{\text{FB},\tau}(\omega)$	-2.102 ± 0.849	-2.455 ± 0.834	2%

$$F_{L,l}(V) = \frac{\Gamma_{\lambda=0}(B \rightarrow V l \bar{\nu})}{\Gamma(B \rightarrow V l \bar{\nu})}, \quad (20)$$

with λ the helicity of the vector meson $V = \rho, \omega$. As an aside, in the $B \rightarrow (\rho \rightarrow \pi\pi) l \bar{\nu}$ decay, it is well known that the longitudinal polarization of the ρ arises in the differential rate with respect to the pion polar helicity angle, as in Eq. (A10). One may derive a similar result for the ω longitudinal polarization in $B \rightarrow (\omega \rightarrow \pi\pi\pi) l \bar{\nu}$ via the Dalitz-type analysis provided in Appendix A yielding

$$\frac{1}{\Gamma} \frac{d\Gamma}{d \cos \theta_+} = \frac{3}{8} [[1 - F_L(\omega)](1 + \cos^2 \theta_+) + 2F_L(\omega) \sin^2 \theta_+], \quad (21)$$

in which the θ_+ helicity angle defines the angle between the π^+ momentum and the B momentum \mathbf{p}_B in the ω rest frame. Second, we calculate the τ polarization (see, e.g., [2])

$$P_\tau(V) = \frac{\Gamma_+(B \rightarrow V\tau\bar{\nu}) - \Gamma_-(B \rightarrow V\tau\bar{\nu})}{\Gamma_+(B \rightarrow V\tau\bar{\nu}) + \Gamma_-(B \rightarrow V\tau\bar{\nu})}, \quad (22)$$

in which the \pm subscript labels the τ helicity, as well as the forward-backward asymmetry

$$A_{\text{FB},l}(V) = \frac{\Gamma_{[0,1]}(B \rightarrow V l \bar{\nu}) - \Gamma_{[-1,0]}(B \rightarrow V l \bar{\nu})}{\Gamma_{[0,1]}(B \rightarrow V l \bar{\nu}) + \Gamma_{[-1,0]}(B \rightarrow V l \bar{\nu})}, \quad (23)$$

in which $\Gamma_L = \int_L d \cos \theta_l [d\Gamma/d \cos \theta_l]$. The predicted central values and uncertainties for these observables are shown in Table V. Using the fitted form factors improves the prediction for these angular observables over using the LCSR fit results alone by up to 21%.

We may further use our combined fit to examine the effects of NP operators defined in Eq. (4) on $B \rightarrow V\tau\bar{\nu}$ decays. (These effects are the same for either ρ or ω —both are vector mesons—up to small differences from their slightly different masses and their disparate decay modes.) As an example, in Fig. 5 we show the variation in $R(\rho)$ for the leptoquark simplified model R_2 [43,44]. In this model, a heavy TeV-scale leptoquark mediator induces nonzero c_{SL} and c_T NP Wilson coefficients constrained such that $c_{\text{SL}} \simeq 8c_T$ once Fierz relations and RG evolution effects are included. Over the range of NP couplings considered, $R(\rho)$ varies by almost a factor of 2.

In Fig. 6 for the benchmark choice $c_{\text{SL}} = 8c_T = 1$, we show the effects on the differential distributions in missing mass squared M_{miss}^2 and the electron momentum p_e from the τ decay compared to the SM. These spectra are generated using the HAMMER library [23,24] to reweight a sample of 5×10^4 events generated with EVTGEN R01-07-00 [45]. We have imposed a common experimental threshold that the lepton momentum be greater than 300 MeV, but otherwise we do not consider reconstruction effects. At the

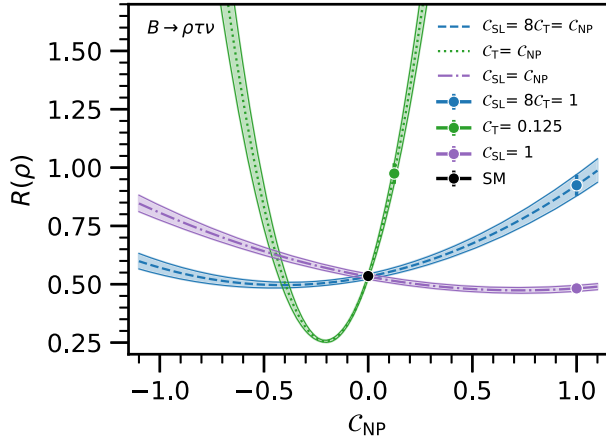


FIG. 5. The impact on the lepton universality ratio $R(\rho)$ for the leptoquark model R_2 , with Wilson coefficients $c_{SL} \simeq 8c_T$. Additionally, the individual contributing NP currents to R_2 are shown. The highlighted NP points correspond to the benchmark points for Fig. 6.

benchmark point, the R_2 couplings generate deviations of approximately 5%–10% compared with the SM distributions. Just as for the analyses of $b \rightarrow c\tau\bar{\nu}$ decays, using the full differential information is expected to provide greater sensitivity to NP effects than considering deviations in $R(V)$ [or $R(\pi)$] alone. Moreover, once high-precision measurements for these decays are available, self-consistent analyses, using, e.g., reweighting tools, may be required to avoid biases in NP interpretations of future anomalous $R(V)$ measurements (if any) [23].

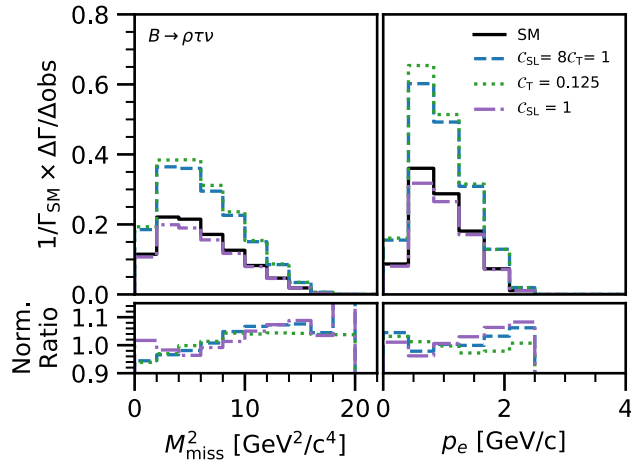


FIG. 6. The $B \rightarrow \rho\tau\bar{\nu}$ distribution in the missing mass squared M_{miss}^2 variable (left) and the lepton momentum in the B rest frame (right) without reconstruction effects, for the R_2 leptoquark model benchmark point $c_{SL} = 8c_T = 1$, and the individual currents at the benchmark points $c_{SL} = 1$ and $c_T = 0.125$. The differential distributions are normalized with respect to the SM rate and include a cut on the electron momentum in the lab frame $p_e > 300$ MeV. In the lower panels, we show the ratio of the shapes of differential distributions, with all distributions normalized to unity.

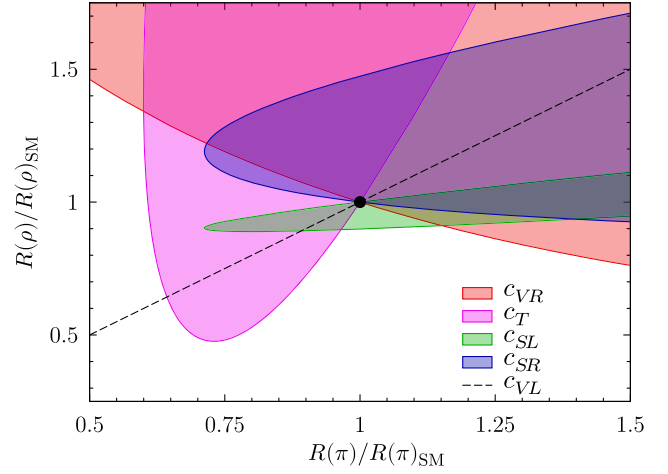


FIG. 7. Allowed regions in the $R(\rho)/R(\rho)_{\text{SM}}$ versus $R(\pi)/R(\pi)_{\text{SM}}$ plane, for each of the (complex) NP couplings c_{SR} , c_{SL} , c_{VR} , and c_T combined with the SM contribution. The coupling c_{VL} simply rescales the SM, and therefore spans only a straight line contour.

Finally, it is perhaps also instructive to characterize the interplay between $R(V)$ and $R(\pi)$: Unlike for $B \rightarrow D^{(*)}$, there are no heavy quark symmetry relations between the vector and pseudoscalar meson decay modes. To this end, in Fig. 7 we show the allowed regions in the $R(\rho)$ – $R(\pi)$ plane, for each of the (complex) couplings c_{SR} , c_{SL} , c_{VR} , and c_T . For the $R(\pi)$ NP predictions, we use the LCSR fit of Ref. [46]. However, we note the SM prediction therefrom is $R(\pi)_{\text{SM}} = 0.75 \pm 0.02$, which is quite different from the SM prediction from the combination of LQCD calculations and experimental data $R(\pi)_{\text{SM}} = 0.641 \pm 0.016$ [3]. (A more recent analysis using LCSR inputs yields 0.688 ± 0.014 [5], which is still in some tension.) For this reason, in Fig. 6 we plot $R(\rho)/R(\rho)_{\text{SM}}$ and $R(\pi)/R(\pi)_{\text{SM}}$, assuming that any LCSR pulls on $R(\pi)$ approximately factor out of these normalized ratios. The allowed regions for each NP coupling are broadly similar to those in the $R(D)$ – $R(D^*)$ plane (see, e.g., Refs. [47,48]).

VI. SUMMARY AND CONCLUSIONS

Using our generated averages of the $B \rightarrow \rho l \bar{\nu}$ and $B \rightarrow \omega l \bar{\nu}$ differential spectra measured by the Belle and BABAR experiments, we performed a combined fit with LCSR results to obtain improved predictions for the $B \rightarrow V$ form factors, for $V = \rho$ or ω , over the full q^2 range.

With our combined fit results, we extracted $|V_{ub}|$ from the averaged spectra in both decay modes,

$$\begin{aligned} |V_{ub}|_{B \rightarrow \rho l \bar{\nu}} &= (2.96 \pm 0.29) \times 10^{-3}, \\ |V_{ub}|_{B \rightarrow \omega l \bar{\nu}} &= (2.99 \pm 0.35) \times 10^{-3}, \end{aligned} \quad (24)$$

finding $|V_{ub}|$ consistently below other inclusive and exclusive extractions and with smaller uncertainty compared to

previous extractions such as in [11]. We further used our combined fit to calculate the following set of observables in the SM: the lepton universality ratios $R(V)$, the longitudinal polarization fractions $F_{L,l}(V)$, the τ polarization $P_\tau(V)$, and the forward-backward asymmetry $A_{FB,l}(V)$. For these observables, we saw improved precision in the predictions by up to 24% compared to using the LCSR results alone. In addition, we briefly investigated the impact of new physics contributions on $R(V)$ in the $B \rightarrow V$ transitions for all four-Fermi NP operators, as well as examining the impacts on differential rates for a benchmark example using the leptoquark model R_2 .

We look forward to future lattice QCD predictions near zero recoil and beyond, which can provide additional constraints on this combined fit in the high q^2 regime. We also look forward to new measurements of differential spectra for $B \rightarrow V l \bar{\nu}$ from Belle II and LHCb. These measurements might help to resolve the tension seen in the $B \rightarrow \rho l \bar{\nu}$ spectra from Belle and BABAR, and to investigate the consistently smaller values of $|V_{ub}|$ extracted from both channels.

ACKNOWLEDGMENTS

We thank Aoife Bharucha, David Straub, and Roman Zwicky for helpful discussions. F. B. is supported by DFG Emmy-Noether Grant No. BE 6075/1-1 and BMBF Grant No. 05H19PDKB1. M. P. is supported by the Argelander Starter-Kit Grant of the University of Bonn and BMBF Grant No. 05H19PDKB1. D. J. R. is supported in part by the Office of High Energy Physics of the U.S. Department of Energy under Contract No. DE-AC02-05CH11231.

APPENDIX A: AMPLITUDES AND DIFFERENTIAL RATES

We write explicit expressions for the $\bar{b} \rightarrow \bar{u}$ amplitudes rather than $b \rightarrow u$, defining the basis of NP operators to be

$$\text{SM: } 2\sqrt{2}V_{ub}^* G_F [\bar{b}\gamma^\mu P_L u] [\bar{\nu}\gamma_\mu P_L l], \quad (\text{A1a})$$

$$\begin{aligned} \text{Vector: } & 2\sqrt{2}V_{ub}^* G_F [\bar{b}(\alpha_L^V \gamma^\mu P_L + \alpha_R^V \gamma^\mu P_R) u] \\ & \times [\bar{\nu}(\beta_L^V \gamma_\mu P_L + \beta_R^V \gamma_\mu P_R) l], \end{aligned} \quad (\text{A1b})$$

$$\begin{aligned} \text{Scalar: } & -2\sqrt{2}V_{ub}^* G_F [\bar{b}(\alpha_L^S P_L + \alpha_R^S P_R) u] \\ & \times [\bar{\nu}(\beta_L^S P_R + \beta_R^S P_L) l], \end{aligned} \quad (\text{A1c})$$

$$\begin{aligned} \text{Tensor: } & -2\sqrt{2}V_{ub}^* G_F [(\bar{b}\alpha_R^T \sigma^{\mu\nu} P_R u)(\bar{\nu}\beta_L^T \sigma_{\mu\nu} P_R l) \\ & + (\bar{b}\alpha_L^T \sigma^{\mu\nu} P_L u)(\bar{\nu}\beta_R^T \sigma_{\mu\nu} P_L l)], \end{aligned} \quad (\text{A1d})$$

with $l = e, \mu, \tau$. The subscript of the β coupling denotes the ν chirality and the subscript of the α coupling is that of the u quark. Operators for the CP conjugate $b \rightarrow u$ processes follow by Hermitian conjugation. The correspondence

between the α, β coefficients and the basis typically chosen, e.g., for $b \rightarrow c$ or $b \rightarrow u$ operators can be found in Ref. [49]. With respect to the notation in Eq. (4),

$$\begin{aligned} c_{SR}^* &= -\alpha_L^S \beta_L^S, & c_{SL}^* &= -\alpha_R^S \beta_L^S, \\ c_{VR}^* &= \alpha_R^V \beta_L^V, & c_{VL}^* &= \alpha_R^V \beta_L^V, \\ c_T^* &= -\alpha_R^T \beta_L^T. \end{aligned} \quad (\text{A2})$$

The $B \rightarrow V l \bar{\nu}$ decay has three external quantum numbers: $\lambda_V = \pm, 0$, $s_l = 1, 2$, and $s_\nu = \pm$, which are the vector meson and massive lepton spin and neutrino helicity, respectively. (We label the s_l spin by “1” and “2,” rather than “−” and “+,” to match the conventions of Ref. [48] for massive spinors on internal lines.) Helicity angles are similarly defined with respect to the $\bar{b} \rightarrow \bar{u}$ process; definitions for the conjugate process follow simply by replacing all particles with their antiparticles. The azimuthal helicity angle ϕ_l of the $\mathbf{p}_l - \mathbf{k}_{\bar{\nu}}$ plane defined in the $l \bar{\nu}$ center-of-mass frame is unphysical in the pure $B \rightarrow V l \bar{\nu}$ decay. See Fig. 8. The single physical polar helicity angle θ_l defines the orientation of \mathbf{p}_l in the lepton center-of-mass reference frame, with respect to $-\mathbf{p}_B$.

For compact expression of the amplitudes, it is further convenient to define

$$\begin{aligned} \hat{q}^2 &= q^2/m_B^2, & r_l &= m_l/m_B, \\ r_V &= m_V/m_B, & |\bar{p}_V| &= |p_V|/m_B, \end{aligned} \quad (\text{A3})$$

in which the spatial momentum $|p_V| = m_V \sqrt{w^2 - 1}$ is the momentum of the vector meson in the B rest frame.

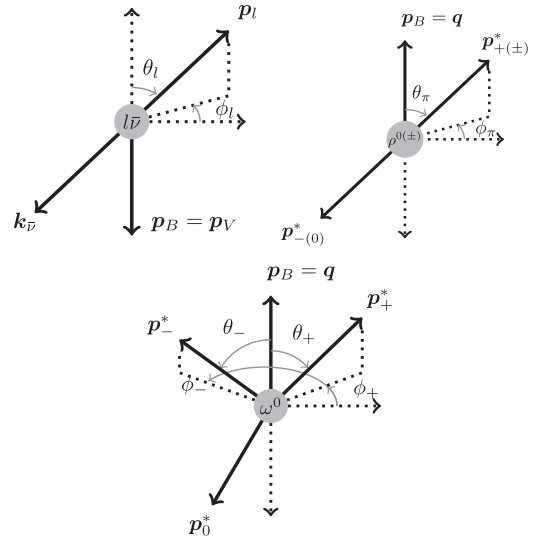


FIG. 8. Definition of the helicity angles in the lepton system ρ and ω rest frames. In the case of the $\rho^0 \rightarrow \pi^+ \pi^-$ ($\rho^\pm \rightarrow \pi^\pm \pi^0$) decay, the helicity angles θ_π and ϕ_π are defined with respect to the π^+ (π^\pm).

We remove an overall prefactor $2c_V G_F V_{ub}^* m_B^2 \sqrt{\hat{q}^2 - r_l^2}$ from the amplitudes, in which the coefficient $c_V = 1/\sqrt{2}$ for the neutral unflavored mesons final states ρ^0 and ω^0 , while $c_V = 1$ for ρ^\pm . Thus, the $B \rightarrow V l \bar{\nu}$ full differential rate

$$\frac{d^2\Gamma}{dq^2 d\cos\theta_l} = \frac{c_V^2 G_F^2 |V_{ub}|^2 m_B^3}{64\pi^3} |\bar{p}_V| \frac{(\hat{q}^2 - r_l^2)^2}{\hat{q}^2} \sum_{\lambda_V, s_l, s_\nu} |A_{\lambda_V s_l s_\nu}|^2 \quad (\text{A4})$$

and the $\bar{b} \rightarrow \bar{u} l \nu$ amplitudes are correspondingly

$$A_{-1} = \sin\theta_l \left\{ -\frac{V(1 + (\alpha_L^V + \alpha_R^V)\beta_L^V)|\bar{p}_V| r_l}{\sqrt{\hat{q}^2}(1 + r_V)} - \frac{A_1(1 + (\alpha_L^V - \alpha_R^V)\beta_L^V) r_l(1 + r_V)}{2\sqrt{\hat{q}^2}} + \frac{2\alpha_R^T \beta_L^T [T_2 + 2T_1|\bar{p}_V| - T_2 r_V^2]}{\sqrt{\hat{q}^2}} \right\}, \quad (\text{A5a})$$

$$A_{-2} = \cos^2\theta_l \left\{ -\frac{2V(1 + (\alpha_L^V + \alpha_R^V)\beta_L^V)|\bar{p}_V|}{1 + r_V} - A_1(1 + (\alpha_L^V - \alpha_R^V)\beta_L^V)(1 + r_V) + \frac{4\alpha_R^T \beta_L^T r_l [T_2 + 2T_1|\bar{p}_V| - T_2 r_V^2]}{\hat{q}^2} \right\}, \quad (\text{A5b})$$

$$A_{-1} = \sin^2\theta_l \left\{ \frac{2V(\alpha_L^V + \alpha_R^V)\beta_R^V|\bar{p}_V|}{1 + r_V} + A_1(\alpha_L^V - \alpha_R^V)\beta_R^V(1 + r_V) + \frac{4\alpha_R^T \beta_L^T r_l [T_2 - 2T_1|\bar{p}_V| - T_2 r_V^2]}{\hat{q}^2} \right\}, \quad (\text{A5c})$$

$$A_{-2} = \sin\theta_l \left\{ \frac{V(\alpha_L^V + \alpha_R^V)\beta_R^V|\bar{p}_V| r_l}{\sqrt{\hat{q}^2}(1 + r_V)} + \frac{A_1(\alpha_L^V - \alpha_R^V)\beta_R^V r_l(1 + r_V)}{2\sqrt{\hat{q}^2}} + \frac{2\alpha_L^T \beta_R^T [T_2 - 2T_1|\bar{p}_V| - T_2 r_V^2]}{\sqrt{\hat{q}^2}} \right\}, \quad (\text{A5d})$$

$$A_{01} = \left\{ \frac{A_P(-\alpha_L^S + \alpha_R^S)\beta_L^S|\bar{p}_V|}{\sqrt{2}r_V} - \frac{\sqrt{2}(1 + (\alpha_L^V - \alpha_R^V)\beta_L^V) r_l (A_0|\bar{p}_V| - 4A_{12}r_V \cos\theta_l)}{\hat{q}^2} - \frac{8\sqrt{2}T_{23}\alpha_R^T \beta_L^T r_V \cos\theta_l}{1 + r_V} \right\}, \quad (\text{A5e})$$

$$A_{02-} = \sin\theta_l \left\{ -\frac{4\sqrt{2}A_{12}(1 + (\alpha_L^V - \alpha_R^V)\beta_L^V) r_V}{\sqrt{\hat{q}^2}} + \frac{8\sqrt{2}T_{23}\alpha_R^T \beta_L^T r_l r_V}{\sqrt{\hat{q}^2}(1 + r_V)} \right\}, \quad (\text{A5f})$$

$$A_{01} = \sin\theta_l \left\{ \frac{4\sqrt{2}A_{12}(-\alpha_L^V + \alpha_R^V)\beta_R^V r_V}{\sqrt{\hat{q}^2}} - \frac{8\sqrt{2}T_{23}\alpha_L^T \beta_R^T r_l r_V}{\sqrt{\hat{q}^2}(1 + r_V)} \right\}, \quad (\text{A5g})$$

$$A_{02+} = \left\{ \frac{A_P(\alpha_L^S - \alpha_R^S)\beta_R^S|\bar{p}_V|}{\sqrt{2}r_V} + \frac{\sqrt{2}(\alpha_L^V - \alpha_R^V)\beta_R^V r_l (A_0|\bar{p}_V| - 4A_{12}r_V \cos\theta_l)}{\hat{q}^2} - \frac{8\sqrt{2}T_{23}\alpha_L^T \beta_R^T r_V \cos\theta_l}{1 + r_V} \right\}, \quad (\text{A5h})$$

$$A_{+1} = \sin\theta_l \left\{ \frac{V(1 + (\alpha_L^V + \alpha_R^V)\beta_L^V)|\bar{p}_V| r_l}{\sqrt{\hat{q}^2}(1 + r_V)} - \frac{A_1(1 + (\alpha_L^V - \alpha_R^V)\beta_L^V) r_l(1 + r_V)}{2\sqrt{\hat{q}^2}} + \frac{2\alpha_R^T \beta_L^T [T_2 - 2T_1|\bar{p}_V| - T_2 r_V^2]}{\sqrt{\hat{q}^2}} \right\}, \quad (\text{A5i})$$

$$A_{+2} = \sin^2\theta_l \left\{ -\frac{2V(1 + (\alpha_L^V + \alpha_R^V)\beta_L^V)|\bar{p}_V|}{1 + r_V} + A_1(1 + (\alpha_L^V - \alpha_R^V)\beta_L^V)(1 + r_V) + \frac{4\alpha_R^T \beta_L^T r_l [2T_1|\bar{p}_V| + T_2(r_V^2 - 1)]}{\hat{q}^2} \right\}, \quad (\text{A5j})$$

$$A_{+1+} = \cos^2\theta_l \left\{ \frac{2V(\alpha_L^V + \alpha_R^V)\beta_R^V|\bar{p}_V|}{1 + r_V} + A_1(-\alpha_L^V + \alpha_R^V)\beta_R^V(1 + r_V) - \frac{4\alpha_L^T \beta_R^T r_l [T_2 + 2T_1|\bar{p}_V| - T_2 r_V^2]}{\hat{q}^2} \right\}. \quad (\text{A5k})$$

As done in Refs. [48–50], in Eqs. (A5) we have adopted spinor conventions such that unphysical ϕ_l phase is removed from the $\bar{b} \rightarrow \bar{u} l \nu$ amplitude, transferring it to the subsequent τ or V vector meson decays to generate physical phase combinations therein. In particular, if subsequent $V \rightarrow X_1 \dots X_n$ decays are included, one may further define helicity angles ϕ_{ij} with respect to the $X_i - X_j$ plane, such that the twist angle $\phi_l - \phi_{ij}$ becomes a physical phase in the $V \rightarrow X_1 \dots X_n$ amplitude. Similarly, $\tau \rightarrow h\nu$

decays, for h any final state system, feature a helicity angle ϕ_h defined by the h - ν plane, such that $\phi_l - \phi_h$ becomes physical in the τ decay amplitude. With respect to the explicit amplitudes $A_{\lambda_V s_l s_\nu}$ in Eqs. (A5), this phase transference amounts to requiring the inclusion of an additional spinor phase function in the subsequent τ and V decay amplitudes: $h_{s_l s_\nu}^I$ and $h_{\lambda_V}^V$, respectively, that modify the usual phase convention of the τ or V helicity basis. These two functions are defined exhaustively via $h_{11}^I = h_{22}^{I*} = 1$, $h_{12}^I = h_{21}^{I*} = e^{i\phi_l}$, and $h_{\lambda_V}^V = e^{-i\lambda_V \phi_l}$.

To incorporate subsequent $\rho \rightarrow 2\pi$ or $\omega \rightarrow 3\pi$ decays, the full differential rate can be written as

$$d\Gamma = \frac{G_F^2 |V_{ub}|^2 c_V^2 m_B^3}{128\pi^4} |\bar{p}_V| \frac{(\hat{q}^2 - r_7^2)^2}{\hat{q}^2} \times \sum_{s_l s_\nu} |A_{s_l s_\nu}|^2 dq^2 d\Omega_l d\mathcal{P}\mathcal{S}_V, \quad (\text{A6})$$

in which $d\mathcal{P}\mathcal{S}_V$ is the phase space measure of the V decay, and the amplitude for $B \rightarrow (\rho \rightarrow 2\pi)l\bar{\nu}$ or $B \rightarrow (\omega \rightarrow 3\pi)l\bar{\nu}$ decomposes in the narrow-width approximation as

$$A_{s_l s_\nu} = \sum_{\lambda_V} \frac{A_{\lambda_V s_l s_\nu} A_{\lambda_V}^V}{\sqrt{2m_V \Gamma_V}}. \quad (\text{A7})$$

The $\rho \rightarrow \pi\pi$ strong decay is generated via the chiral interaction $g_{\rho\rho\mu}[\pi(\partial^\mu\pi) - (\partial^\mu\pi)\pi]$. In the $\rho^0 \rightarrow \pi^+\pi^-$ ($\rho^- \rightarrow \pi^-\pi^0$) decay, we denote the momentum of the π^+ (π^-) in the ρ^0 (ρ^-) rest frame by \mathbf{p}_+^* (\mathbf{p}_-^*), with magnitude $|p_\pi^*|$. In our phase conventions, the $\rho \rightarrow \pi\pi$ amplitude is then

$$A_\pm^\rho = -g_\rho \sqrt{2} |p_\pi^*| e^{\pm i(\phi_\pi - \phi_l)} \sin \theta_\pi, \quad (\text{A8a})$$

$$A_0^\rho = 2g_\rho |p_\pi^*| \cos \theta_\pi, \quad (\text{A8b})$$

in which the helicity angles θ_π and ϕ_π define the orientation of \mathbf{p}_+^* (\mathbf{p}_-^*) with respect to $+\mathbf{p}_B$ in the ρ^0 (ρ^-) rest frame. See Fig. 8. Note that the physical twist angle $\phi_\pi - \phi_l$ appears.

Combining Eq. (A7) with Eqs. (A5) and (A8) yields the full amplitude expressions, from which square matrix elements follow immediately. The phase space measure of the $\rho \rightarrow \pi\pi$ decay is trivially

$$d\mathcal{P}\mathcal{S}_\rho = \frac{|p_\pi^*|}{16\pi^2 m_\rho} d\Omega_\pi, \quad (\text{A9})$$

over which integration of the square amplitudes is straightforward. [One finds $\Gamma[\rho \rightarrow \pi\pi] = g_\rho^2 |p_\pi^*|^3 / (2\pi m_\rho^2)$.] From Eqs. (A8), one may also immediately derive the differential decay in the cascade $B \rightarrow (\rho \rightarrow \pi\pi)l\nu$,

$$\frac{1}{\Gamma} \frac{d\Gamma}{d \cos \theta_\pi} = \frac{3}{2} \left[[1 - F_L(\rho)] \frac{\sin^2 \theta_\pi}{2} + F_L(\rho) \cos^2 \theta_\pi \right], \quad (\text{A10})$$

in which $F_L(\rho)$ is the longitudinal polarization (20).

The $\omega \rightarrow \pi^+\pi^-\pi^0$ strong decay is generated via the interaction $g_\omega e^{\mu\nu\rho\sigma} \omega_\mu \partial_\nu \pi \partial_\rho \pi \partial_\sigma \pi$. For the $\omega \rightarrow \pi^+\pi^-\pi^0$ decay, we denote the momenta of the π^\pm in the ω rest frame by \mathbf{p}_\pm^* , with magnitude $|p_\pm^*|$, respectively. In our phase conventions, the $\omega \rightarrow \pi^+\pi^-\pi^0$ decay amplitude is then

$$A_\pm^\omega = \frac{g_\omega m_\omega |p_+^*| |p_-^*|}{\sqrt{2}} [e^{\pm i(\phi_\pm - \phi_l)} \cos \theta_\mp \sin \theta_\pm - e^{\pm i(\phi_\mp - \phi_l)} \cos \theta_\pm \sin \theta_\mp], \quad (\text{A11a})$$

$$A_0^\omega = i g_\omega m_\omega |p_+^*| |p_-^*| \sin(\phi_+ - \phi_-) \sin \theta_+ \sin \theta_-. \quad (\text{A11b})$$

Here the helicity angles θ_\pm and ϕ_\pm define the orientation of \mathbf{p}_\pm^* with respect to $+\mathbf{p}_B$ in the ω rest frame. See Fig. 8. Note that two physical twist angles $\phi_\pm - \phi_l$ appear.

Combining Eq. (A7) with Eqs. (A5) and (A11) yields the full amplitude expressions. However, for the $\omega \rightarrow 3\pi$ decay, the orientations of \mathbf{p}_\pm^* cannot be chosen freely simultaneously because $p_\omega - p_+ - p_- = p_0$ is constrained to be on the π^0 mass shell. That is, one cannot simply integrate the square amplitude arising from Eq. (A11) over $d\Omega_+ d\Omega_-$, because the integration limits become nontrivial.

Natural coordinates for integration of the $\pi^+\pi^-\pi^0$ phase space may instead be constructed by defining relative polar coordinates θ_{+-} and ϕ_{+-} , e.g., for the π^- with respect to the π^+ , in the usual spirit of a Dalitz-style analysis. In particular, we choose coordinates as shown in Fig. 9, such that the \hat{z} axis aligns with \mathbf{p}_+^* and the \hat{y} axis lies in the x - y plane, at $-\phi_+$ from the y axis. The latter defines the

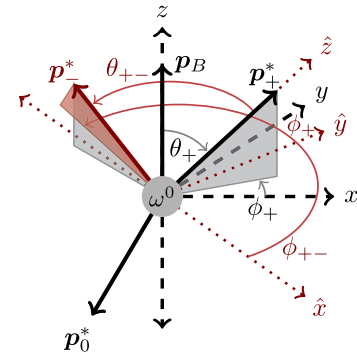


FIG. 9. Definition of the relative helicity angles θ_{+-} and ϕ_{+-} with respect to the hatted coordinate system shown in red, in the ω rest frame. The \hat{z} axis aligns with \mathbf{p}_+^* ; the \hat{y} axis lies in the x - y plane at $-\phi_+$ from the y axis. The latter defines the orientation of the azimuthal angle ϕ_{+-} of \mathbf{p}_-^* around \mathbf{p}_+^* . The polar angle θ_{+-} is simply the angle between \mathbf{p}_+^* and \mathbf{p}_-^* .

azimuthal angle ϕ_{+-} of \mathbf{p}_-^* around \mathbf{p}_+^* , while θ_{+-} is the angle between \mathbf{p}_+^* and \mathbf{p}_-^* . Because $d\Omega_+ d\Omega_- = d\Omega_+ d\Omega_{+-}$, the phase space measure becomes

$$d\mathcal{PS}_\omega = \frac{dE_+^* dE_-^*}{8(2\pi)^5} d\Omega_+ d\phi_{+-}, \quad (\text{A12})$$

with the mass-shell constraint

$$2|p_+^*||p_-^*| \cos \theta_{+-} = m_\omega^2 + 2m_+^2 - m_0^2 - 2m_\omega(E_+^* + E_-^*) + 2E_+^* E_-^*, \quad (\text{A13})$$

in which E_\pm^* are the energies of the π^\pm in the ω rest frame, and m_+ and m_0 are the π^\pm and π^0 masses, respectively. The integration domain of $dE_+^* dE_-^*$ is nontrivial. However, defining $s = (p_+ + p_-)^2$ and $\mathcal{E}^\pm = E_\pm^* \pm E_-^*$, the measure can be further rewritten

$$d\mathcal{PS}_\omega = \frac{ds d\mathcal{E}^-}{32m_\omega(2\pi)^5} d\Omega_+ d\phi_{+-}, \quad (\text{A14})$$

in which the ordered integration domain $4m_+^2 \leq s \leq (m_\omega - m_0)^2$ and $-\mathcal{E}_{\max}^-(s) \leq \mathcal{E}_- \leq \mathcal{E}_{\max}^-(s)$ with

$$\begin{aligned} \mathcal{E}^+(s) &= \frac{m_\omega^2 - m_0^2 + s}{2m_\omega}, \\ \mathcal{E}_{\max}^-(s) &= [(s - 4m_+^2)(\mathcal{E}^+(s)^2/s - 1)]^{1/2}. \end{aligned} \quad (\text{A15})$$

In these polar coordinates, the $\omega \rightarrow \pi^+ \pi^- \pi^0$ helicity amplitudes become

$$A_\pm^\omega = \mp \frac{g_\omega m_\omega |p_+^*||p_-^*|}{\sqrt{2}} e^{\pm i(\phi_+ - \phi_-)} \times [\cos \phi_{+-} \pm i \cos \theta_+ \sin \phi_{+-}] \sin \theta_{+-}, \quad (\text{A16a})$$

$$A_0^\omega = -i g_\omega m_\omega |p_+^*||p_-^*| \sin(\phi_{+-}) \sin \theta_+ \sin \theta_{+-}. \quad (\text{A16b})$$

Noting further from Eq. (A13),

$$|p_+^*|^2 |p_-^*|^2 \sin^2 \theta_{+-} = \frac{s}{4} [\mathcal{E}_{\max}^-(s)^2 - (\mathcal{E}^-)^2], \quad (\text{A17})$$

integration of the square of the amplitudes over $d\mathcal{PS}_\omega$ is now straightforward. [One finds $\Gamma[\omega \rightarrow 3\pi] \simeq 1.94 \times 8 / (6\pi^3) g_\omega^2 m_\omega^7$.] One may also immediately derive the differential decay in the cascade $B \rightarrow (\omega \rightarrow \pi\pi\pi) l \bar{\nu}$,

$$\frac{1}{\Gamma} \frac{d\Gamma}{d\cos\theta_+} = \frac{3}{8} [[1 - F_L(\omega)](1 + \cos^2\theta_+) + 2F_L(\omega) \sin^2\theta_+] \quad (\text{A18})$$

in which $F_L(\omega)$ is the longitudinal polarization of the ω .

APPENDIX B: CORRELATIONS

We give the postfit correlation matrices for the spectrum average discussed in Sec. III in Tables VI and VII. The postfit correlation matrices for the form factor fits discussed in Sec. IV are provided in Tables VIII and IX.

TABLE VI. Correlation matrix of the averaged $B \rightarrow \rho l \bar{\nu}$ spectrum.

	[0, 2]	[2, 4]	[4, 6]	[6, 8]	[8, 10]	[10, 12]	[12, 14]	[14, 16]	[16, 18]	[18, 20]	[20, 22]
[0, 2]	1.00	-0.30	0.03	0.01	0.09	0.09	0.09	0.09	0.08	0.08	0.02
[2, 4]	-0.30	1.00	-0.03	0.09	0.11	0.12	0.12	0.12	0.11	0.10	0.02
[4, 6]	0.03	-0.03	1.00	-0.18	0.13	0.13	0.15	0.14	0.13	0.12	0.03
[6, 8]	0.01	0.09	-0.18	1.00	0.06	0.18	0.18	0.18	0.16	0.14	0.04
[8, 10]	0.09	0.11	0.13	0.06	1.00	-0.21	0.05	0.04	0.12	0.10	0.03
[10, 12]	0.09	0.12	0.13	0.18	-0.21	1.00	-0.00	0.07	0.15	0.13	0.04
[12, 14]	0.09	0.12	0.15	0.18	0.05	-0.00	1.00	-0.16	0.14	0.12	0.04
[14, 16]	0.09	0.12	0.14	0.18	0.04	0.07	-0.16	1.00	0.10	0.14	0.05
[16, 18]	0.08	0.11	0.13	0.16	0.12	0.15	0.14	0.10	1.00	-0.27	-0.11
[18, 20]	0.08	0.10	0.12	0.14	0.10	0.13	0.12	0.14	-0.27	1.00	-0.13
[20, 22]	0.02	0.02	0.03	0.04	0.03	0.04	0.04	0.05	-0.11	-0.13	1.00

TABLE VII. Correlation matrix of the averaged $B \rightarrow \omega l \bar{\nu}$ spectrum.

	[0, 4]	[4, 8]	[8, 10]	[10, 12]	[12, 21]	θ_2	θ_5
[0, 4]	1.00	-0.15	0.08	0.04	0.06	-0.01	0.00
[4, 8]	-0.15	1.00	0.09	0.09	0.15	-0.01	-0.00
[8, 10]	0.08	0.09	1.00	-0.01	0.12	-0.00	-0.00
[10, 12]	0.04	0.09	-0.01	1.00	0.15	0.00	-0.00
[12, 21]	0.06	0.15	0.12	0.15	1.00	-0.00	-0.00
θ_2	-0.01	-0.01	-0.00	0.00	-0.00	1.00	0.00
θ_5	0.00	-0.00	-0.00	-0.00	-0.00	0.00	1.00

TABLE VIII. Correlation matrix for $|V_{ub}|$ and the BSZ parameters to the averaged $B \rightarrow \rho l \bar{\nu}$ spectrum and the LCSR data.

	$ V_{ub} $	$\alpha_1^{A_0}$	$\alpha_2^{A_0}$	$\alpha_0^{A_1}$	$\alpha_1^{A_1}$	$\alpha_2^{A_1}$	$\alpha_0^{A_{12}}$	$\alpha_1^{A_{12}}$	$\alpha_2^{A_{12}}$	α_0^V	α_1^V	α_2^V	$\alpha_0^{T_1}$	$\alpha_1^{T_1}$	$\alpha_2^{T_1}$	$\alpha_1^{T_2}$	$\alpha_2^{T_2}$	$\alpha_0^{T_{23}}$	$\alpha_1^{T_{23}}$	$\alpha_2^{T_{23}}$
$ V_{ub} $	1.00	-0.05	-0.02	-0.54	0.07	0.05	-0.75	-0.08	0.04	-0.53	0.09	-0.02	-0.50	0.10	-0.03	0.08	0.07	-0.55	-0.11	-0.01
$\alpha_1^{A_0}$	-0.05	1.00	-0.15	0.06	0.14	0.20	0.30	0.86	0.81	-0.03	0.22	0.16	-0.04	0.24	0.12	0.15	0.27	0.26	0.86	0.73
$\alpha_2^{A_0}$	-0.02	-0.15	1.00	0.02	0.14	0.28	-0.07	-0.23	-0.19	-0.02	0.06	0.57	-0.17	0.06	0.56	0.11	0.44	-0.03	0.07	0.40
$\alpha_0^{A_1}$	-0.54	0.06	0.02	1.00	0.56	0.46	0.29	0.02	-0.15	0.90	0.54	-0.31	0.88	0.54	-0.33	0.55	0.38	0.24	0.20	0.09
$\alpha_1^{A_1}$	0.07	0.14	0.14	0.56	1.00	0.87	-0.13	0.08	-0.04	0.48	0.95	-0.24	0.45	0.95	-0.28	0.98	0.79	-0.06	0.23	0.18
$\alpha_2^{A_1}$	0.05	0.20	0.28	0.46	0.87	1.00	-0.12	0.12	0.08	0.37	0.88	0.02	0.31	0.88	-0.03	0.87	0.94	-0.04	0.28	0.32
$\alpha_0^{A_{12}}$	-0.75	0.30	-0.07	0.29	-0.13	-0.12	1.00	0.44	0.26	0.28	-0.15	0.06	0.26	-0.15	0.07	-0.13	-0.14	0.69	0.32	0.12
$\alpha_1^{A_{12}}$	-0.08	0.86	-0.23	0.02	0.08	0.12	0.44	1.00	0.89	-0.05	0.19	-0.06	-0.02	0.21	-0.09	0.09	0.11	0.25	0.80	0.59
$\alpha_2^{A_{12}}$	0.04	0.81	-0.19	-0.15	-0.04	0.08	0.26	0.89	1.00	-0.234	0.09	0.04	-0.19	0.11	-0.00	-0.01	0.10	0.08	0.60	0.57
α_0^V	-0.53	-0.03	-0.02	0.90	0.48	0.37	0.28	-0.05	-0.23	1.00	0.54	-0.37	0.90	0.48	-0.34	0.50	0.31	0.23	0.11	-0.00
α_1^V	0.09	0.22	0.06	0.54	0.95	0.88	-0.15	0.19	0.09	0.54	1.00	-0.33	0.48	0.97	-0.36	0.96	0.80	-0.11	0.29	0.22
α_2^V	-0.02	0.16	0.57	-0.31	-0.24	0.02	0.06	-0.06	0.04	-0.37	-0.33	1.00	-0.47	-0.32	0.96	-0.29	0.22	0.15	0.24	0.52
$\alpha_0^{T_1}$	-0.50	-0.04	-0.17	0.88	0.45	0.31	0.26	-0.02	-0.19	0.90	0.48	-0.47	1.00	0.51	-0.53	0.50	0.23	0.20	0.07	-0.10
$\alpha_1^{T_1}$	0.10	0.24	0.06	0.54	0.95	0.88	-0.15	0.21	0.11	0.48	0.97	-0.32	0.51	1.00	-0.39	0.98	0.82	-0.10	0.31	0.24
$\alpha_2^{T_1}$	-0.03	0.12	0.56	-0.33	-0.28	-0.03	0.07	-0.09	-0.00	-0.34	-0.36	0.96	-0.53	-0.39	1.00	-0.34	0.15	0.17	0.20	0.47
$\alpha_1^{T_2}$	0.08	0.15	0.11	0.55	0.98	0.87	-0.13	0.09	-0.01	0.50	0.96	-0.29	0.50	0.98	-0.34	1.00	0.81	-0.07	0.23	0.18
$\alpha_2^{T_2}$	0.07	0.27	0.44	0.38	0.79	0.94	-0.14	0.11	0.10	0.31	0.80	0.22	0.23	0.82	0.15	0.81	1.00	-0.04	0.36	0.50
$\alpha_0^{T_{23}}$	-0.55	0.26	-0.03	0.24	-0.06	-0.04	0.69	0.25	0.08	0.23	-0.11	0.15	0.20	-0.10	0.17	-0.07	-0.04	1.00	0.32	0.11
$\alpha_1^{T_{23}}$	-0.11	0.86	0.07	0.20	0.23	0.28	0.32	0.80	0.60	0.11	0.29	0.24	0.07	0.31	0.20	0.23	0.36	0.32	1.00	0.86
$\alpha_2^{T_{23}}$	-0.01	0.73	0.40	0.09	0.18	0.32	0.12	0.59	0.57	-0.00	0.22	0.52	-0.10	0.24	0.47	0.18	0.50	0.11	0.86	1.00

TABLE IX. Correlation matrix for $|V_{ub}|$ and the BSZ parameters to the averaged $B \rightarrow \omega l \bar{\nu}$ spectrum and the LCSR data.

	$ V_{ub} $	$\alpha_1^{A_0}$	$\alpha_2^{A_0}$	$\alpha_0^{A_1}$	$\alpha_1^{A_1}$	$\alpha_2^{A_1}$	$\alpha_0^{A_{12}}$	$\alpha_1^{A_{12}}$	$\alpha_2^{A_{12}}$	α_0^V	α_1^V	α_2^V	$\alpha_0^{T_1}$	$\alpha_1^{T_1}$	$\alpha_2^{T_1}$	$\alpha_1^{T_2}$	$\alpha_2^{T_2}$	$\alpha_0^{T_{23}}$	$\alpha_1^{T_{23}}$	$\alpha_2^{T_{23}}$
$ V_{ub} $	1.00	-0.22	0.08	-0.48	0.04	0.04	-0.80	-0.28	-0.20	-0.46	0.06	-0.04	-0.43	0.06	-0.05	0.05	0.05	-0.61	-0.24	-0.19
$\alpha_1^{A_0}$	-0.22	1.00	-0.48	0.12	0.04	0.03	0.47	0.93	0.85	0.05	0.11	0.08	0.08	0.14	0.03	0.04	0.08	0.49	0.92	0.81
$\alpha_2^{A_0}$	0.08	-0.48	1.00	0.03	0.05	0.10	-0.27	-0.52	-0.39	0.07	-0.01	0.18	-0.02	-0.02	0.21	0.05	0.16	-0.30	-0.40	-0.10
$\alpha_0^{A_1}$	-0.48	0.12	0.03	1.00	0.61	0.46	0.24	0.05	-0.10	0.94	0.60	-0.46	0.93	0.61	-0.48	0.61	0.45	0.26	0.21	0.13
$\alpha_1^{A_1}$	0.04	0.04	0.05	0.61	1.00	0.84	-0.08	-0.02	-0.24	0.59	0.97	-0.51	0.58	0.97	-0.55	0.99	0.81	-0.02	0.12	-0.05
$\alpha_2^{A_1}$	0.04	0.03	0.10	0.46	0.84	1.00	-0.07	-0.00	-0.13	0.41	0.87	-0.16	0.40	0.86	-0.22	0.84	0.95	-0.02	0.09	0.01
$\alpha_0^{A_{12}}$	-0.80	0.47	-0.27	0.24	-0.08	-0.07	1.00	0.59	0.46	0.21	-0.10	0.12	0.20	-0.09	0.13	-0.09	-0.08	0.76	0.47	0.32
$\alpha_1^{A_{12}}$	-0.28	0.93	-0.52	0.05	-0.02	-0.00	0.59	1.00	0.89	-0.01	0.06	0.05	0.02	0.08	0.01	-0.02	0.01	0.51	0.89	0.75
$\alpha_2^{A_{12}}$	-0.20	0.85	-0.39	-0.10	-0.24	-0.13	0.46	0.89	1.00	-0.16	-0.14	0.19	-0.13	-0.12	0.16	-0.22	-0.10	0.36	0.70	0.73
α_0^V	-0.46	0.05	0.07	0.94	0.59	0.41	0.21	-0.01	-0.16	1.00	0.61	-0.52	0.93	0.59	-0.50	0.60	0.41	0.21	0.14	0.07
α_1^V	0.06	0.11	-0.01	0.60	0.97	0.87	-0.10	0.06	-0.14	0.61	1.00	-0.52	0.59	0.99	-0.56	0.98	0.85	-0.03	0.18	0.01
α_2^V	-0.04	0.08	0.18	-0.46	-0.51	-0.16	0.12	0.05	0.19	-0.52	-0.52	1.00	-0.54	-0.51	0.95	-0.53	-0.07	0.13	0.08	0.30
$\alpha_0^{T_1}$	-0.43	0.08	-0.02	0.93	0.58	0.40	0.20	0.02	-0.13	0.93	0.59	-0.54	1.00	0.62	-0.60	0.61	0.39	0.21	0.15	0.04
$\alpha_1^{T_1}$	0.06	0.14	-0.02	0.61	0.97	0.86	-0.09	0.08	-0.12	0.59	0.99	-0.51	0.62	1.00	-0.58	0.99	0.85	-0.02	0.21	0.03
$\alpha_2^{T_1}$	-0.05	0.03	0.21	-0.48	-0.55	-0.22	0.13	0.01	0.16	-0.50	-0.56	0.95	-0.60	-0.58	1.00	-0.59	-0.13	0.11	0.03	0.26
$\alpha_1^{T_2}$	0.05	0.04	0.05	0.61	0.99	0.84	-0.09	-0.02	-0.22	0.60	0.98	-0.53	0.61	0.99	-0.59	1.00	0.82	-0.03	0.12	-0.05
$\alpha_2^{T_2}$	0.05	0.08	0.16	0.45	0.81	0.95	-0.08	0.01	-0.10	0.41	0.85	-0.07	0.39	0.85	-0.13	0.82	1.00	-0.02	0.16	0.13
$\alpha_0^{T_{23}}$	-0.61	0.49	-0.30	0.26	-0.02	-0.02	0.76	0.51	0.36	0.21	-0.03	0.13	0.21	-0.02	0.11	-0.03	-0.02	1.00	0.53	0.32
$\alpha_1^{T_{23}}$	-0.24	0.92	-0.40	0.21	0.12	0.09	0.47	0.89	0.70	0.14	0.18	0.08	0.15	0.21	0.03	0.12	0.16	0.53	1.00	0.86
$\alpha_2^{T_{23}}$	-0.19	0.81	-0.10	0.13	-0.05	0.01	0.32	0.75	0.73	0.07	0.01	0.30	0.04	0.03	0.26	-0.05	0.13	0.32	0.86	1.00

- [1] Y. S. Amhis *et al.* (HFLAV Collaboration), *Eur. Phys. J. C* **81**, 226 (2021).
- [2] F. U. Bernlochner, M. F. Sevilla, D. J. Robinson, and G. Wormser, [arXiv:2101.08326](https://arxiv.org/abs/2101.08326).
- [3] F. U. Bernlochner, *Phys. Rev. D* **92**, 115019 (2015).
- [4] D. Bečirević, F. Jaffredo, A. Peñuelas, and O. Sumensari, *J. High Energy Phys.* **05** (2021) 175.
- [5] D. Leljak, D. van Dyk, and B. Melić, *J. High Energy Phys.* **07** (2021) 036.
- [6] P. Hamer *et al.* (Belle Collaboration), *Phys. Rev. D* **93**, 032007 (2016).
- [7] P. del Amo Sanchez *et al.* (BABAR Collaboration), *Phys. Rev. D* **83**, 032007 (2011).
- [8] J. P. Lees *et al.* (BABAR Collaboration), *Phys. Rev. D* **87**, 032004 (2013); **87**, 099904(E) (2013).
- [9] A. Sibidanov *et al.* (Belle Collaboration), *Phys. Rev. D* **88**, 032005 (2013).
- [10] A. Biswas, S. Nandi, S. K. Patra, and I. Ray, [arXiv:2103.01809](https://arxiv.org/abs/2103.01809).
- [11] A. Bharucha, D. M. Straub, and R. Zwicky, *J. High Energy Phys.* **08** (2016) 098.
- [12] L. Cao *et al.* (Belle Collaboration), *Phys. Rev. D* **104**, 012008 (2021).
- [13] B. O. Lange, M. Neubert, and G. Paz, *Phys. Rev. D* **72**, 073006 (2005).
- [14] P. Gambino, P. Giordano, G. Ossola, and N. Uraltsev, *J. High Energy Phys.* **10** (2007) 058.
- [15] J. R. Andersen and E. Gardi, *J. High Energy Phys.* **01** (2006) 097.
- [16] E. Gardi, *Frascati Phys. Ser.* **47**, 381 (2008), <https://inspirehep.net/literature/789304>.
- [17] U. Aglietti, F. Di Lodovico, G. Ferrera, and G. Ricciardi, *Eur. Phys. J. C* **59**, 831 (2009).
- [18] U. Aglietti, G. Ferrera, and G. Ricciardi, *Nucl. Phys.* **B768**, 85 (2007).
- [19] P. Colangelo, F. De Fazio, and F. Lopalco, *Phys. Rev. D* **100**, 075037 (2019).
- [20] F. U. Bernlochner, Z. Ligeti, and S. Turczyk, *Phys. Rev. D* **90**, 094003 (2014).
- [21] G. Banelli, R. Fleischer, R. Jaarsma, and G. Tetlalmatzi-Xolocotzi, *Eur. Phys. J. C* **78**, 911 (2018).
- [22] C.-H. Chen and S.-h. Nam, *Phys. Lett. B* **666**, 462 (2008).
- [23] F. U. Bernlochner, S. Duell, Z. Ligeti, M. Papucci, and D. J. Robinson, *Eur. Phys. J. C* **80**, 883 (2020).
- [24] F. U. Bernlochner, S. Duell, Z. Ligeti, M. Papucci, and D. J. Robinson, HAMMER—Helicity Amplitude Module for Matrix Element Reweighting, 2020.
- [25] X.-W. Kang, B. Kubis, C. Hanhart, and U.-G. Meißner, *Phys. Rev. D* **89**, 053015 (2014).
- [26] A. Khodjamirian, T. Mannel, and N. Offen, *Phys. Rev. D* **75**, 054013 (2007).
- [27] C. Beleño *et al.* (Belle Collaboration), *Phys. Rev. D* **103**, 112001 (2021).
- [28] A. Sirlin, *Nucl. Phys.* **B196**, 83 (1982).
- [29] S. L. Tostado and G. López Castro, *Eur. Phys. J. C* **76**, 495 (2016).
- [30] G. Isidori, S. Nabeebaccus, and R. Zwicky, *J. High Energy Phys.* **12** (2020) 104.
- [31] C. Boyd, B. Grinstein, and R. F. Lebed, *Nucl. Phys.* **B461**, 493 (1996).
- [32] C. Boyd, B. Grinstein, and R. F. Lebed, *Phys. Rev. D* **56**, 6895 (1997).
- [33] C. Bourrely, I. Caprini, and L. Lellouch, *Phys. Rev. D* **79**, 013008 (2009); **82**, 099902(E) (2010).
- [34] S. Aoki *et al.* (Flavour Lattice Averaging Group), *Eur. Phys. J. C* **80**, 113 (2020).
- [35] I. Balitsky, V. Braun, and A. Kolesnichenko, *Nucl. Phys.* **B312**, 509 (1989).
- [36] V. M. Braun and I. E. Filyanov, *Z. Phys. C* **44**, 157 (1989).
- [37] V. Chernyak and I. Zhitnitsky, *Nucl. Phys.* **B345**, 137 (1990).
- [38] P. Ball, V. M. Braun, and H. G. Dosch, *Phys. Rev. D* **44**, 3567 (1991).
- [39] P. Ball and R. Zwicky, *Phys. Rev. D* **71**, 014029 (2005).
- [40] A. Bharucha, *J. High Energy Phys.* **05** (2012) 092.
- [41] M. Freytsis, Z. Ligeti, and J. T. Ruderman, *Phys. Rev. D* **92**, 054018 (2015).
- [42] F. U. Bernlochner and Z. Ligeti, *Phys. Rev. D* **95**, 014022 (2017).
- [43] I. Doršner, S. Fajfer, A. Greljo, J. F. Kamenik, and N. Košnik, *Phys. Rep.* **641**, 1 (2016).
- [44] W. Buchmüller, R. Rckl, and D. Wyler, *Phys. Lett. B* **191**, 442 (1987).
- [45] D. J. Lange, *Nucl. Instrum. Methods Phys. Res., Sect. A* **462**, 152 (2001).
- [46] N. Gubernari, A. Kokulu, and D. van Dyk, *J. High Energy Phys.* **01** (2019) 150.
- [47] M. Tanaka and R. Watanabe, *Phys. Rev. D* **87**, 034028 (2013).
- [48] Z. Ligeti, M. Papucci, and D. J. Robinson, *J. High Energy Phys.* **01** (2017) 083.
- [49] F. U. Bernlochner, Z. Ligeti, and D. J. Robinson, *Phys. Rev. D* **97**, 075011 (2018).
- [50] F. U. Bernlochner, Z. Ligeti, D. J. Robinson, and W. L. Sutcliffe, *Phys. Rev. Lett.* **121**, 202001 (2018).